Modeling of time-lapse seismic reflection data from CO_2 sequestration at West Pearl Queen Field

SAND2007-2926C

Lewis C. Bartel, Matthew M. Haney, David F. Aldridge, Neill P. Symons, and Gregory J. Elbring

Geophysics Department, Sandia National Laboratories, Albuquerque, New Mexico

Introduction

Sequestration of CO_2 in depleted oil reservoirs, saline aquifers, or unminable coal sequences may prove to be an economical and environmentally safe means for long-term removal of carbon from the atmosphere. Requirements for storage of CO_2 in subsurface geologic repositories (e.g., less than 0.1% per year leakage) pose significant challenges for geophysical remote sensing techniques. The many issues relevant to successful CO_2 sequestration (volume in place, migration, leakage rate) require improved understanding of the advantages and pitfalls of potential monitoring methods. Advanced numerical modeling of time-lapse seismic reflection responses offers a controlled environment for testing hypotheses and exploring alternatives. The U.S. Department of Energy has conducted CO_2 sequestration and monitoring tests at West Pearl Queen (WPQ) field in southeastern New Mexico (see below, Figure A). High-quality 9C/3D seismic reflection data were acquired before and after injection of ~2 kt of CO_2 into a depleted sandstone unit at ~4200 ft depth. Images developed from time-lapse seismic data appear to reveal strong reflectivity changes attributed to displacement of brine by CO_2 (see below, Figure B). We are pursuing seismic numerical modeling studies with the goal of understanding and assessing the reliability and robustness of the time-lapse reflection responses.

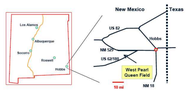

Figure A. Location of sequestration project near Hobbs, New Mexico.

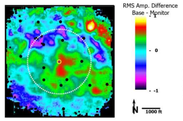

Figure B. Difference in RMS seismic amplitudes between baseline and monitor surveys on top of the Queens formation in map view (Benson and Davis, 2005). The zone of high positive amplitude near the center of the survey is interpreted to be due to the injected CO_2 at the West Pearl Queen Field.

Seismic model construction

Well log information is used to construct a preliminary one-dimensional (1D) layered model for the WPQ site, prior to introduction of CO2 (Figure 1). The CO2 sequestration reservoir is the Shattuck sandstone member of the Queen formation (a Central Basin Platform dolomite with numerous intrabedded sands), occupying the depth interval ~1365 m to ~1383 m below surface. After CO2 injection, seismic wavespeeds are reduced by ~5-6%, as suggested by laboratory measurements tabulated in Wang et al. (1998). Mass density of the CO2-saturated sandstone is estimated by assuming complete replacement of brine pore fluid by CO2 with a medium of porosity $\phi = 0.16$ (Figure 2). The vertical variation in compressional (P) wavespeed Vp, shear (S) wavespeed Vs, and mass density ρ are subsequently extended to 3D numerical grids for use in the FD wave propagation algorithm. Figure 3 illustrates a 3D post-CO2-injection P-wave speed model, where a uniform reduction in Vp is distributed within a 300 m × 600 m rectangular zone centered on the injector well.

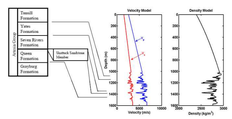

Figure 1. Vertical profiles of compressional wavespeed (Vp), shear wavespeed (Vs), and mass density (ρ) developed for the WPQ field CO2 sequestration site. Well log information from the Stivason #4 well is used to construct these profiles over the depth interval ~1025 m to ~1550 m. Compressional wavespeed is then linearly extrapolated to the surface such that the normal incidence P-P reflection traveltime from the Queen formation is ~0.640 seconds. Shear wavespeed profile in the overburden is obtained by linearly extrapolating the logged value at top of Yates formation to the surface value Vs = 0.5971 Vp. Finally, overburden mass density is generated via a Gardner-style relation. Depths of top of Yates, Seven Rivers, Queen, and Grayburg formations in the Central Basin Platform stratigraphic column are indicated. The Shattuck Sandstone member of the upper Queen formation is identified by a prominent kick (toward lower values) of Vp, Vs, and ρ.

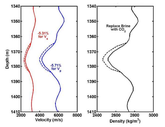

Figure 2. Pre-CO2-injection (solid) and post-CO2-injection (dashed) depth logs of compressional wavespeed (Vp), shear wavespeed (Vs), and mass density (ρ) in the Queen sand formation. Reductions in these elastic parameters due to CO2 injection are confined to the Shattuck Sandstone unit.

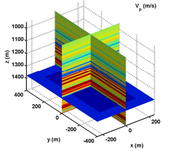

Figure 3. Three-dimensional view of the P-wave speed (Vp) distribution in the vicinity of the CO2 injection wellbore located at (x, y) = (0, 0) m. The horizontal plane at depth z = 1378 m (in the Shattuck Sandstone unit) depicts a uniformly-distributed ~5.7% reduction in Vp inside a rectangular zone with lateral extent Δx = 300 m and Δy = 600 m.

Velocity-Stress Elastodynamic System and Finite-Difference Grid

Nine, coupled, first-order, non-homogeneous, partial differential equations:

$$\frac{\partial \mathbf{v}}{\partial t} - b\left(\nabla \cdot \boldsymbol{\sigma}\right) = b\left(\mathbf{f} + \nabla \cdot \mathbf{m}_a\right)$$

$$\frac{\partial \boldsymbol{\sigma}}{\partial t} - \lambda\left(\nabla \cdot \mathbf{v}\right)\mathbf{I} - \mu\left(\nabla \mathbf{v} + \nabla \mathbf{v}^{\mathrm{T}}\right) = \frac{\partial \mathbf{m}_s}{\partial t}$$

Wavefield Variables:
$\mathbf{v}(\mathbf{x},t)$ - velocity vector
$\boldsymbol{\sigma}(\mathbf{x},t)$ - stress tensor

Elastic Earth Model Parameters:
$\lambda(\mathbf{x})$, $\mu(\mathbf{x})$ - Lamé coefficients
$b(\mathbf{x})$ - mass buoyancy

Seismic Body Sources:
$\mathbf{f}(\mathbf{x},t)$ - force density vector
$\mathbf{m}(\mathbf{x},t)$ - moment density tensor

Staggered Spatial Grid

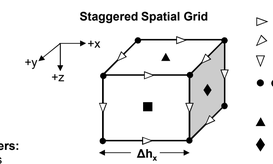

Staggered Temporal Grid

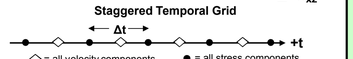

3D velocity-stress system is numerically solved with an explicit, time-domain, O(2,4) staggered-grid, FD algorithm

Sandia National Laboratories is a multiprogram science and engineering facility operated by Sandia Corporation, a Lockheed-Martin Company, for the US Department of Energy under contract DE-AC04-94AL85000.

Seismic data modeling

Synthetic seismic data are calculated with a time-domain, finite-difference (FD) numerical algorithm, appropriate for 3D wave propagation within a heterogeneous and isotropic elastic medium. All of the common seismological phases (P-waves, S-waves, reflections, refractions, mode-conversions, primaries, multiples, surface waves, diffractions, scattered arrivals, etc) are simulated with fidelity, provided spatial and temporal grid intervals are sufficiently fine. The large scale of these simulations mandates use of a massively-parallel computational implementation of the algorithm. The 3D numerical grid used for FD modeling consists of 351 × 501 × 803 ≈ 141.2 million gridpoints with spatial intervals $\Delta x = \Delta y = \Delta z = 2$ m. Seismic trace duration is 1.5 s, equivalent to 15,001 FD timesteps with a temporal interval $\Delta t = 0.1$ ms.

Figure 4 depicts a small portion of the field data acquisition geometry of the WPQ field time-lapse seismic surveys. A complete computational replication of the seismic data generated by all of these sources is beyond the scope of the current investigation. Rather, we calculate five gathers of seismic traces generated by the particular sources indicated by large red dots in Figure 4. Each source is modeled as a buried vertical force (1 m deep), and the source waveform is a Ricker wavelet with peak frequency 25 Hz (1% amplitude bandwidth ~1-70 Hz). Receivers are three-component (3C) particle velocity sensors, also emplaced 1 m below the horizontal stress-free surface of the earth.

Synthetic seismic data are generated for both the pre-CO2-injection and post-CO2-injection earth models. At normal plot scales, only subtle differences in the calculated traces are discernable. However, after subtracting the traces, the expression of the CO2-altered zone at depth is quite evident. Figure 5 displays the difference (post-injection *minus* pre-injection) of the vertical component (Vz) seismograms recorded by a central north-south (y-direction) line of 81 receivers; the seismic energy source is positioned at (x, y) = (0, -400) m (lower large red dot in Figure 4). The strong event with zero-offset arrival time ~0.640 s is due to CO2-alteration. All seismic reflections from interfaces above this zone (as well as horizontally-propagating surface waves, and many FD grid boundary reflections) disappear in the subtraction process.

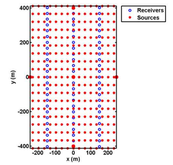

Figure 4. Surface deployment of seismic energy sources (red dots) and receivers (blue dots) in the vicinity of the CO2 injector wellhead for the WPQ field time-lapse seismic reflection surveys. Injector well is located at coordinate origin. The five large red dots indicate energy sources used to calculate synthetic seismic reflection data for subsequent reverse time migrations.

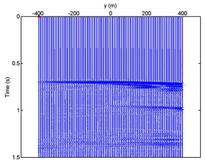

Figure 5. Synthetic seismic reflection data calculated with a 3D time-domain finite-difference (FD) elastic wave propagation algorithm. Traces depict the *difference* (post-CO2-injection minus pre-CO2-injection) in vertical particle velocity (Vz) recorded at surface receivers. The seismic energy source (red dot) is positioned at (x, y) = (0, -400) m, and the line of 81 receivers extends from (x, y) = (0, -400) m to (x, y) = (0, +400) m in Figure 4.

Migration of synthetic seismic data

Images of the CO2-altered zone at depth are formed by *migrating* the synthetic seismic reflection data with a 3D elastic reverse time migration (RTM) algorithm. This algorithm is designed to propagate surface-recorded seismic trace data downward into a numerical model of the earth's subsurface. Two such subsurface wavefields are generated: one is activated at the seismic energy source, and the other at the set of receivers that record data from this particular source. The zero-time-lag cross-correlation of these two wavefields provides an image of subsurface reflectivity. Compositing of images from many seismic sources (five in our case) improves image quality by enhancing coherent signal and suppressing migration artifacts.

We apply reverse time migration to the synthetic seismic data generated from both the pre-injection and post-injection models of the WPQ CO2 sequestration site. Figure 6 illustrates *time-lapse* images on selected horizontal planes within the Shattuck sandstone unit of the Queen formation. Each image is obtained by subtracting the pre-CO2-injection migrated image from the corresponding post-CO2-injection image. There is a clear response due to CO2-alteration of elastic parameters. Although this response is (correctly) centered on the injector well, edge definition is diffuse and ambiguous (compare time-lapse images with the uniformly distributed rectangular Vp-reduction zone in the lower right panel of Figure 6).

A similar synthetic modeling and migration experiment has been performed with a spatially-variable CO2-altered zone within the Shattuck sandstone. A 3D fractal distribution of elastic parameters (Figures 7 and 8) mimics a geologically-realistic sinuous channel sand environment within the Queen formation. These channels may form preferred flow pathways for the injected CO2. A comparison of time-lapse migrated images on the same depth plane for the fractal and uniform reductions in elastic parameters is illustrated in Figure 9. Clearly, the fractal distribution reduces the overall amplitude of the image response, as well as introducing an asymmetry related to the underlying geometry of the medium parameters. The 3D image comparison illustrated in Figure 10 also indicates lower-amplitude response associated with the fractal model.

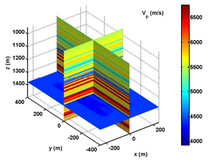

Figure 8. Three-dimensional view of post-CO2-injection fractal P-wave speed (Vp) distribution. Only subtle reductions in Vp are discernable on the horizontal plane at depth z = 1378 m. Compare this image with the uniform reduction in Vp displayed in Figure 3 (and plotted with an identical color scale).

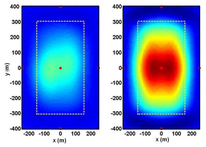

Figure 9. Comparison of time-lapse migrated images on the horizontal plane with depth z = 1404 m. Each panel depicts the difference (post-CO2-injection *minus* pre-CO2-injection) in reverse-time-migrated elastic wavefields on the image plane. Left panel is constructed from synthetic seismic reflection data generated with the 3D fractal distribution of elastic parameters (Vp, Vs, ρ) within the CO2-alteration zone. Right panel is obtained from seismic data calculated with the uniform distribution of elastic properties. The dashed rectangle delineates the lateral extent of the CO2-alteration zone within the Shattuck Sandstone. Seismic reflection data are calculated for five energy sources located on the surface at the red dots. As expected, the amplitude of the time-lapse image generated from the fractal model is reduced, compared with the uniform model. Additionally, a slight asymmetry is discernable in the image from the fractal model.

Static shift experiments

Highly repeatable field data acquisition parameters and conditions are essential for effective time-lapse seismic reflection surveying. In order to correctly interpret the processed seismic data, all observed changes in the data should be attributed to changes in subsurface earth properties that take place between surveys. However, as a practical matter, it is difficult to exactly replicate the original source and receiver locations and earth coupling conditions on the second seismic survey. Additionally, changes in the shallow subsurface weathered zone, generated say by increased/decreased moisture content, may obscure a proper interpretation of the time-lapse data. We examine these effects by introducing static time shifts into the post-injection seismic data generated from the uniformly-distributed (Vp, Vs, ρ) CO2-alteration model. These shifts are designed to simulate data differences arising from the aforementioned effects. The 2D spatial distribution of the time shifts mimics a realistic *surface consistent* static situation: all traces generated from the same source location are shifted by an identical amount, and all traces recorded at the same receiver location are shifted by an identical (but different) amount. Time shifts are drawn from a zero-mean, rectangular random distribution with specified maximum value.

Figure 11 displays time-lapse migrated images resulting from this study. Clearly, larger magnitude shifts lead to a progressive degradation in image quality, in both amplitude and shape. With time shifts as large as 5% (of the one-way traveltime through an assumed shallow subsurface weathered zone), the resulting time-lapse image on the horizontal plane with the Shattuck sandstone becomes uninterpretable. Finally, Figure 12 clearly indicates that time shifts lead to a significant degradation in image quality throughout the 3D image volume. Our conclusion is that variations between the two field surveys must be minimized during data acquisition, and that the time-lapse seismic data must be carefully processed to eliminate any residual differences not attributable to the changed earth model.

Figure 11. Time-lapse migration images on a horizontal plane at depth z = 1404 m, generated by applying random time shifts to the post-injection seismic reflection traces. These static shifts are designed to simulate spatially-distributed perturbations present in the post-injection survey, arising from differences in source and receiver placement or earth coupling, or variations within the shallow subsurface weathered zone. Random time shifts are drawn from a zero-mean rectangular probability distribution, with maximum value equal to a specified percentage of one-way traveltime through an assumed 200 m thick weathered zone. Clearly, larger magnitude shifts result in a progressive degradation of image quality. As indicated previously, the red dots denote locations of five seismic energy sources used to generate the synthetic seismic reflection data, and the dashed rectangle outlines the CO2-alteration zone within the Shattuck Sandstone.

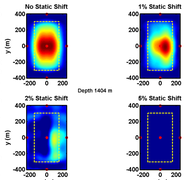

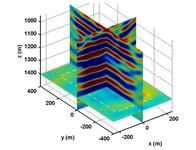

Figure 12. Three-dimensional view of the time-lapse migration volume generated from the post-injection seismic reflection dataset with 2% static time shifts applied. The horizontal plane at depth z = 1404 m is located within the Shattuck Sandstone CO2-injection zone; dashed rectangle outlines the extent of spatially-uniform alteration in elastic medium parameters (Vp, Vs, ρ). The static shifts create a significant degradation in image quality *throughout* the 3D volume. In particular, a large-amplitude oscillatory response (red/blue = positive/negative) is evident above the CO2 injection zone.

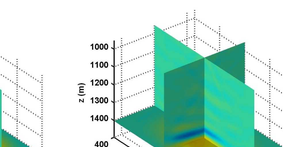

Figure 6. Comparison of *time-lapse migration images* on three different horizontal planes located within the CO2 injection formation. Each image is obtained by subtracting the pre-CO2-injection migrated wavefield from the post-CO2-injection migrated wavefield. The three images are plotted with the same color amplitude scale (red/blue = positive/negative). Lower right panel illustrates a uniform reduction in P-wave speed on the horizontal plane at depth z = 1378 m. Ideally, the time-lapse images should coincide with this rectangle. Differences arise from the small number of seismic energy sources and receivers utilized in the reverse-time-migrations, their restricted spatial aperture, and the limited spectral bandwidth of the propagating seismic waves.

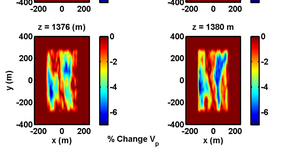

Figure 7. Percent change in P-wave speed (Vp) for a fractal distribution model on four horizontal planes within the Shattuck Sandstone unit of the Queen formation. Spatially-variable reductions in Vp are confined to a rectangular zone with lateral dimensions Δx = 300 m and Δy = 600 m.

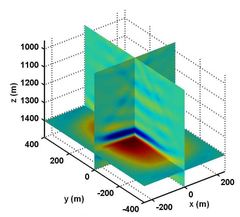

Figure 10. Comparison of three-dimensional time-lapse migration images for the uniform CO2-alteration model (left) and the fractal CO2-alteration model (right). Both images are plotted with the same color amplitude scale, with green indicating null (i.e., zero difference). Clearly, the uniform distribution model generates a larger amplitude response on the horizontal plane at depth z = 1404 m.

Layered medium modeling

Since the stratigraphy at WPQ field (and indeed most of the Permian Basin of West Texas and Southeast New Mexico) is well-approximated by a sequence of horizontal layers, we are currently developing a fast forward modeling code that exploits advantages in modeling for 1D layered media. This capability enables rapid calculation of, for instance, amplitude vs. offset (AVO) seismic reflection responses in a single-processor workstation computational environment. AVO analysis of seismic reflections is widely practiced in the petroleum industry, and is used to infer lithologic and/or fluid saturation parameters of a petroleum reservoir. Although the specialization to a 1D layered earth model is a restriction, it allows exploitation of efficient numerical procedures enabling extremely rapid calculations. Seismic wavefield simulations can be conducted in a matter of minutes, rather than hours.

A example source gather of pressure traces, calculated for an identical earth model and recording geometry used for a run with the 3D FD algorithm, is displayed in Figure 14. Apart from a very small amplitude imbalance, the traces illustrated in Figures 13 and 14 are virtually identical. This provides assurance that our two computational algorithms are valid. The current algorithm implementation utilizes acoustic (i.e., ideal fluid) layers. Future plans are to upgrade the approach to accommodate solid elastic layers, so that shear and mode-converted seismic phases can be accurately modeled.

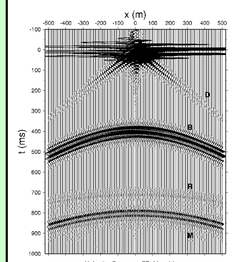

Figure 13. Source gather of pressure traces calculated with 3D velocity-pressure finite-difference acoustic wave propagation algorithm. Seismic energy source is an explosion located 10 m below the surface; 101 pressure receivers are deployed from -500 m to +500 m, and located 5 m below surface. Note direct arrival (D), prominent reflection (B), reflected arrival from a subsurface horizontal interface (R), and a free surface multiple (M). Extremely large pressure amplitudes are obvious at receivers near the source. No time- or space-varying plot gain is applied.

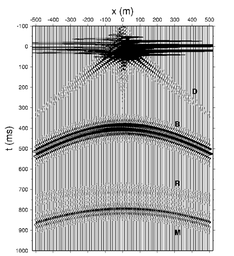

Figure 14. Example source gather of pressure traces calculated with 1D layered-medium acoustic wave propagation algorithm. Earth model and data recording configuration is exactly the same as for Figure 13. Expect for a small difference in overall amplitude level, these traces are virtually identical to those displayed in Figure 13 (and calculated by an entirely different numerical algorithm).

Discussion, Conclusions, Future directions

Utilizing a 3D time-domain finite-difference isotropic elastic wave propagation algorithm, we are capable of generating realistic synthetic data at WPQ field. With this capability, we examine how various types of errors and noise in the 4D data degrade the ability to image a deep CO2 plume. Source/receiver sampling, subsurface illumination, correlated geologic heterogeneity, and static shifts are considered. As a result, we are able to make quantitative estimates of the tolerable errors for monitoring CO2 injection at WPQ field. Due to the strong sensitivity of the time-lapse images on statics errors, some receivers used for CO2 monitoring may need to be located below the complex and variable near-surface layer. We plan in the future to consider fully 9C time-lapse data (which exists at WPQ) in the numerical modeling, as well as statistical models of the Shattuck Sandstone to more realistically represent reservoir complexity.

Ultimately, we intend to simulate seismic reflection data at the WPQ field CO2 sequestration site with a *poroelastic* wave propagation algorithm, based on Biot's dynamic equations governing wave propagation within a fluid-saturated porous solid. This algorithm, also developed in the SNL Geophysics Department, allows quantitative prediction of effects on seismic data due to various subsurface fluid and flow parameters such as porosity, fluid type, saturation, permeability, pore structure tortuosity, fluid viscosity, etc, without resorting to effective medium elastic assumptions. Since numerical solution of Biot's poroelastic equations is considerably more demanding than in elastodynamics, our massively-parallel version of the velocity-stress-pressure finite-difference algorithm (Aldridge *et al.*, 2005) must be employed.

REFERENCES

Aldridge, D.F., Symons, N.P. and Bartel, L.C., 2005, Poroelastic wave propagation with a velocity-stress-pressure algorithm: Poromechanics III, Proceedings of the Third International Conference on Poromechanics, University of Oklahoma, Norman, OK, 24-27 May 2005, pages 253-258.

Benson, R. D. and Davis, T. L., 2005, CO_2 Sequestration in a Depleted Oil Reservoir – West Pearl Queen Field: 67th EAGE Conference and Exhibition, June 13-16, Madrid, Spain, P37.

Malaver, C., 2004, Statistical Applications to Quantitative Seismic Reservoir Characterization and Monitoring at West Pearl Queen Field, Lea County, New Mexico: MSc. Thesis, Colorado School of Mines.

Wang, Z., Cates, M.E., and Langan, R.T., 1998, Seismic monitoring of a CO_2 flood in a carbonate reservoir: a rock physics study: Geophysics, **63**, 1604-1617.